

1
2
3
4
5
6
7
8
9
10
11
12
13
14
15
16
17
18
19
20
21
22
23
24
25
26
27
28
29
30
31
32
33
34
35
36
37
38

**Atmospheric circulation patterns associated to the variability of River
Ammer floods: evidence from observed and proxy data**

N. Rimbu¹, M. Czymzik^{2,3}, M. Ionita^{1,4}, G. Lohmann^{1,4}, and A. Brauer²

¹Alfred Wegener Institute Helmholtz Centre for Polar and Marine Research, Bremerhaven, Germany

²GFZ German Research Centre for Geosciences, Climate Dynamics and Landscape Evolution, Potsdam,
Germany

³Lund University, Department of Geology, Lund, Sweden

⁴MARUM – Center for Marine Environmental Sciences, University of Bremen, Bremen, Germany

Correspondence to: N. Rimbu (norel.rimbu@awi.de)

39 **Abstract**

40 The relationship between the frequency of River Ammer floods (southern Germany) and atmospheric
41 circulation variability is investigated based on observational Ammer discharge data back to 1926 and a
42 flood layer time series from varved sediments of the downstream Lake Ammersee for the pre-
43 instrumental period back to 1766. A composite analysis reveals that, at synoptic time scales, observed
44 River Ammer floods are associated with enhanced moisture transport from the Atlantic Ocean and the
45 Mediterranean towards the Ammer region, a pronounced trough over Western Europe as well as
46 enhanced potential vorticity at upper levels. We argue that this synoptic scale configuration can trigger
47 heavy precipitation and floods in the Ammer region. Interannual to multidecadal increases in flood
48 frequency, as recorded in the instrumental discharge record, are associated to a wave-train pattern
49 extending from the North Atlantic to western Asia with a prominent negative center over western
50 Europe. A similar atmospheric circulation pattern is associated with increases in flood layer frequency
51 in the Lake Ammersee sediment record during the pre-instrumental period. We argue that the complete
52 flood layer time-series from Lake Ammersee sediments covering the last 5500 years, contains
53 information about atmospheric circulation variability on inter-annual to millennial time-scales.

54

55

56

57

58

59

60

61

62

63

64 **1. Introduction**

65 Flood events are natural disasters which cause important economic losses. Therefore, the variability
66 and predictability of flood occurrences have been addressed in many research studies (e.g. Jacobeit et
67 al., 2003; Czymzik et al., 2010; Peña et al., 2015; Schillereff et al., 2014; Ionita et al., 2008, 2015).

68 Recent studies (Corella et al., 2014, and reference therein) identified pronounced temporal variability in
69 the occurrence of heavy precipitation and flood events using instrumental and environmental proxy
70 time series. For example, during the last decades, the frequency of heavy precipitation in central
71 Europe increased (Zolina et al., 2008) while winter precipitation extremes in coastal Mediterranean
72 sites decreased (Toreti et al., 2010). On longer time-scales, flood frequency in different parts of Europe
73 is characterized by distinct multi-decadal to centennial variability (Czymzik et al., 2010; Corella et al.,
74 2014). Understanding flood responses to climate forcing is essential to anticipate possible changes in
75 flood dynamics related to anthropogenic climate change.

76 The present study focuses on flood variability of River Ammer, located in the northern pre-alpine
77 region. Heavy precipitation variability in the alpine region has been related to various internal or
78 external forcing on different scales. On the mesoscale, atmospheric flow is strongly influenced by local
79 topography triggering convective precipitation. On the synoptic-scale, high potential vorticity
80 intrusions over Western Europe play an important role in the forcing of heavy precipitation along the
81 southern Alpine rim (Schlemmer et al., 2010, and references therein). Furthermore, heavy precipitation
82 and floods in the Ammer region are related to large-scale circulation patterns. Czymzik et al. (2010)
83 related major River Ammer floods (southern Germany) to the occurrence of particular flood-prone
84 weather regimes. Glur et al. (2013) associate flood frequency increases in the alpine realm to periods of
85 colder climate with a higher occurrence of westerly and Vb tracks. Toreti et al. (2013) show that the
86 occurrence of debris flows in the Swiss Alps is connected to two synoptic atmospheric circulation
87 patterns which favor anomalous southerly flow towards this area and high potential instability. Inter-

88 annual to multi-decadal variability of heavy precipitation and flood events in the alpine region are also
89 related to large-scale atmospheric teleconnection patterns. Peña et al. (2015) emphasized the role of the
90 Summer North Atlantic Oscillation (SNAO) in generating flood variability in Swiss rivers. The East
91 Atlantic (EA) pattern and SNAO modify the frequency of atmospheric circulation patterns controlling
92 debris flow occurrences in the Swiss Alps (Toreti et al., 2013). Flood frequency variability in the pre-
93 Alps on multi-decadal time-scales was further related to changes in solar activity (Czymzik et al., 2010;
94 Peña et al., 2015).

95 In this study we investigate the relationship between the frequency of River Ammer floods and
96 atmospheric circulation. Identifying the atmospheric mechanisms behind River Ammer floods allows a
97 better interpretation of the flood layer record from varved Lake Ammersee sediments reaching back the
98 last 5500 years (Czymzik et al., 2010, 2013). Flood layers form during Ammer River floods, when
99 detrital catchment material is eroded, transported into the lake and deposited on the lake floor when
100 transport capacity of the inflowing turbidity diminishes in the water body. Here we use both,
101 instrumental River Ammer discharge and Lake Ammersee flood layer data in combination with long-
102 term observed and reconstructed climatic fields to investigate the relationship between River Ammer
103 flood frequency and atmospheric circulation. This will improve the interpretation of River Ammer
104 flood frequency changes as presented in previous studies (e.g. Czymzik et al., 2010).

105 The paper is organized as follows. Data and methods are presented in Section 2. The main results
106 follow in Section 3. In Section 3.1 the synoptic scale patterns that cause River Ammer floods are
107 presented. The atmospheric circulation pattern associated to inter-annual to multi-decadal increases in
108 River Ammer flood frequency during the observational period are presented in Section 3.2. The
109 atmospheric circulation patterns associated with flood layer frequency increases during the
110 instrumental and pre-instrumental period, with focus on the similarity with the corresponding patterns

111 derived from observational data, are described in Section 3.3. A discussion and the main conclusions
112 follow in Section 4.

113 **2. Data and methods**

114 River Ammer rises in the Bavarian Alps, southern Germany, (Fig. 1a) and flows northward to Lake
115 Ammersee (Czymzik et al., 2010). The river is relatively small (84 km length) and has a catchment area
116 of ~ 700 km². The Ammer catchment is located in the transition zone between maritime North Atlantic
117 and continental climate influenced by both frequent cyclonic westerly airflow and atmospheric
118 blocking through high-pressure fields (Petrow and Merz, 2009). The annual Ammer flow regime is
119 characterized by strong seasonal variations with a maximum during late spring and summer (Czymzik
120 et al., 2010).

121 The main quantity analyzed here is the mean daily Ammer River runoff recorded at gauge Weilheim
122 (Bayerisches Landesamt für Umwelt, 2007) during the period 1926 to 2006. Although River Ammer
123 floods occur mainly from May to August (Czymzik et al., 2010; Ludwig et al., 2013), we analyze the
124 runoff data within entire year. As a proxy for River Ammer floods in the pre-instrumental period, we
125 used the flood layer record from Lake Ammersee described in Czymzik et al. (2010, 2013). This record
126 was downloaded from the online environmental data base PANGAEA (www.pangaea.de).

127 The atmospheric circulation patterns associated to River Ammer floods in the instrumental discharge
128 and flood layer record are based on annual mean 500hPa geopotential height (Z500) and 850hPa
129 temperature (T850) anomalies calculated using 20th Century Reanalysis, version 2 (hereafter 20CR)
130 data (Compo et al., 2011) starting in 1871. The temperature pattern associated with River Ammer
131 floods in the discharge record over the period 1926–2006 are based on the University Delaware air
132 temperature and precipitation data set (UDel_AirT_Precip) provided by the NOAA/OAR/ESRL PSD,
133 Boulder, Colorado, USA (available at <http://www.esrl.noaa.gov/psd/>).

134 Also from the 20CR data base we used daily fields of specific humidity (q), zonal (u) and meridional
135 (v) wind. These quantities were used to calculate vertically integrated water vapor transport (IWT) over
136 the period 1926–2006. The magnitude of daily IWT is calculated in an Eulerian frame-work as follows:

$$137 \quad IWT = \left[\left(\int_{1000}^{300} qu \frac{dp}{g} \right)^2 + \left(\int_{1000}^{300} qv \frac{dp}{g} \right)^2 \right]^{1/2}$$

138 where g is the acceleration due to gravity. The vertical integration is limited to the 1000 to 300hPa
139 pressure interval because specific humidity in the 20CR data is negligible above 300hPa. Daily Z500
140 were used to establish the synoptic scale atmospheric circulation pattern associated to high ($>125 \text{ m}^3 \text{ s}^{-1}$)
141 daily Ammer River runoff. The 250hPa divergence field, used to identify regions with anomalous
142 vertical motions, is calculated from the daily 250hPa zonal and meridional wind fields.

143 Daily 200hPa potential vorticity (PV) field, for the period 1979–2006, were obtained from ERA-
144 INTERIM (Dee et al., 2011) database. The upper-level PV anomalies are strongly related to extreme
145 precipitation events (Schlemmer et al., 2010; Krichak et al., 2014) and are used here to find possible
146 atmospheric mechanisms behind River Ammer floods at synoptic time scales.

147 We also use Z500 and air temperature (T) reconstructions for the period 1766 to 1870, extracted from
148 the reconstructed gridded meteorological data set of Casty et al. (2007), to derive flood related patterns
149 prior 20CR data.

150 **3. Results**

151 **3.1 Synoptic scale atmospheric patterns associated to River Ammer floods**

152 The time series of mean daily River Ammer discharge (Fig. 1b) shows no significant linear trend
153 during the period 1926–2006. However, visual inspection of the discharge time-series (Fig. 1b) reveals
154 distinct inter-annual to multi-decadal flood frequency variations. Daily River Ammer discharge ranges
155 between 2.6 and 534.6 $\text{m}^3 \text{ s}^{-1}$. Mean discharge over the analyzed period is 15 $\text{m}^3 \text{ s}^{-1}$, while the lower and
156 upper quartiles are 8.9 and 18.3 $\text{m}^3 \text{ s}^{-1}$ respectively. A discharge of 125 $\text{m}^3 \text{ s}^{-1}$ is considered as threshold

157 for flood layer deposition in the Lake Ammersee sediment record. Above this discharge threshold the
158 deposition of a flood layer during a flood is very likely (Czymzik et al., 2010).

159 During the 81 year period 1926–2006 32 days with River Ammer discharge higher than $125 \text{ m}^3\text{s}^{-1}$ were
160 generated by 20 independent flood events (Fig. 1b). The composite map of daily Z500 anomalies
161 during these River Ammer flood days (Fig. 2a, shaded) shows two centers of positive Z500 anomalies
162 northwest of the Iberian Peninsula and north of the Black Sea and two negative Z500 anomaly centers
163 over the Iceland region and southern Europe. The anomaly pattern (Fig. 2a, shaded) contains elements
164 of the two synoptic patterns associated to debris flows in the Swiss Alps as described by Toreti et al.
165 (2013) (their Fig. 2). The corresponding daily Z500 composite map (Fig. 2a, contours) depicts a wave-
166 like structure with a pronounced trough over western and central Europe as well as two ridges over the
167 eastern North Atlantic and northeastern Europe. The IWT composite map for days with mean daily
168 River Ammer discharge higher than $125 \text{ m}^3\text{s}^{-1}$ (Fig. 2b) depicts enhanced moisture transport from the
169 Atlantic towards to the northern alpine flank. Thereby, the Ammer region is located along the axis of
170 the highest IWT (Fig. 2b). To link this moisture transport to local heavy precipitation a mechanism is
171 needed to lift up the wet air. Previous studies (Browning, 1997; Schlemmer et al., 2010; Krichak et al.,
172 2014) emphasized a strong relationship between PV anomalies and precipitation extremes. Southern
173 intrusions of air with relatively high PV in the upper troposphere or lower stratosphere are commonly
174 accompanied by a local lowering of the tropopause, intense vertical motions, high vertically integrated
175 water vapor transport, rapid cyclogenesis, intense convection and heavy rainfall (e.g. Krichak et al.,
176 2014). Therefore, we investigate the 250hPa atmospheric circulation and 200hPa PV fields associated
177 with flood days with discharge higher than $125 \text{ m}^3\text{s}^{-1}$. The composite map of 250hPa circulation
178 associated with daily River Ammer floods indicates a continuous high speed wind system with two
179 regional maxima in the Atlantic and African region (Fig. 3a). A pronounced convergence zone, which
180 is indicative of descendent motions, is reflected between the exit region of the Atlantic branch and the

181 entrance region of the African branch of the jet (Fig. 3a, dashed contour lines). A pronounced
182 divergence zone is visible above the Ammer region (Fig. 3a, solid contour lines). This is indicative for
183 strong vertical motions and heavy rainfall. The poleward side of a jet exit region is preferred for
184 cyclonic growth, which in turn induces heavy rainfall events (Hoskins et al., 1978). A similar synoptic
185 pattern was found to be responsible for high streamflow anomalies of the Rhine River (Ionita et al.,
186 2012). Consistent with Fig. 3a, a region of relatively high PV is identified at 200hPa level (Fig. 3b).
187 Both divergence (Fig. 3a) and high PV (Fig. 3b) regions are relatively small, consistent with a strong
188 local character of the heavy precipitation events.

189 To better assess the atmospheric circulation patterns associated to River Ammer floods as revealed by
190 the composite analysis, we exemplary investigate the Z500, IWT and PV responses to the River
191 Ammer flood on 19 and 20 July 1981 (Fig. 4). During 19 July 1981 a prominent trough dominates
192 central and western Europe (Fig. 4a). The IWT (Fig. 4b) shows narrow bands over the Northeastern
193 Atlantic and Western Europe, similar to atmospheric rivers (e.g. Lavers et al., 2012). An intrusion of
194 relatively high PV from the north is recorded at the 200hPa level (Fig. 4c). In addition, a relatively
195 narrow stream of high PV flows from the Mediterranean area to central Europe (Fig. 4c). This high PV
196 stream is accompanied by exceptional northward transport of moisture from the Mediterranean (Fig.
197 4b). On 20 July 1981 the axis of the trough above Europe remains in a similar position (Fig. 4d), while
198 the structure of the IWT changes significantly (Fig. 4e) compared to the previous day (Fig. 4b).
199 Furthermore, the high PV center above the Ammer region tends to isolate from the high PV pool at
200 higher latitudes (Fig. 4f). To conclude, the composite situation during the River Ammer flood on 19 an
201 20 July 1981 shares common characteristics with most River Ammer floods $>125\text{m}^3\text{s}^{-1}$ during the
202 period 1926–2006. However, there are also River Ammer floods that are associated to atmospheric
203 circulation patterns and mechanisms different than those presented in this case study. For example, the
204 circulation associated to the River Ammer flood on 14 June 1959 (not shown) is a typical omega

205 blocking circulation with heavy precipitation produced on the eastern side of the block. However, most
206 of the River Ammer floods (discharge $> 125 \text{ m}^3\text{s}^{-1}$) are related to synoptic patterns that are similar to
207 those that characterize the 19 to 20 July 1981 flood, which is consistent with the composite analysis
208 shown in Fig. 2.

209 **3.2 Observed River Ammer flood frequency and atmospheric circulation back to 1926**

210 The annual frequency of River Ammer floods, defined as the number of days when mean daily
211 Ammer River discharge is higher than $125 \text{ m}^3\text{s}^{-1}$, shows pronounced decadal to multi-decadal
212 variability (Fig. 5a) with increased flood frequencies from 1940 to 1960 and during the 1980s and
213 2000s. The composite map of annual Z500 anomalies for the years with River Ammer flood frequency
214 is different from zero (Fig. 5b) shows a spatial structure that bears some similarities with the
215 corresponding synoptic scale pattern (Fig. 2a). Positive Z500 anomalies prevail in the North Atlantic
216 region and northeastern Europe while negative Z500 anomalies dominate over a broad area from
217 Iceland to the Central Mediterranean (Fig. 5b). This Z500 anomaly pattern resembles the dominant
218 atmospheric circulation anomaly pattern associated with the occurrence of debris flows in the southern
219 Swiss Alps as described by Toreti et al. (2013) (their Fig. 2a). The spatial temperature pattern
220 associated with River Ammer floods (Fig. 5c) is consistent with the corresponding atmospheric
221 circulation pattern (Fig. 5a) depicting negative anomalies over central and southern Europe and strong
222 positive anomalies over northeastern Europe.

223 **3.3 Flood layer frequency and atmospheric circulation back to 1766**

224 In the following we investigate the relationship between changes in flood layer frequency in the Lake
225 Ammersee sediment record and atmospheric circulation. The flood layer record used in this study is
226 described in Czymzik et al. (2010). We investigate the atmospheric circulation patterns associated
227 with flood layer variability for the period 1871–1999 using 20CR data and for the period 1766–1870
228 using reconstructed gridded meteorological data (Casty et al., 2007).

229 The Lake Ammersee flood layer record for the period 1871–1999 (Fig. 6a) shows increased flood
230 frequencies in the 1980s and 1950s, comparable to the instrumental River Ammer discharge record in
231 the overlapping parts (Fig. 5a). Older periods of enhanced flood frequency occur during the 1920s and
232 1880s (Fig. 6a). The average Z500 anomalies for all years with a deposited flood layer during this
233 period (Fig. 6b) depicts a pattern similar to that based on the instrumental River Ammer flood record
234 (Fig. 5b). A well-defined wave-train that appears in the 850hPa temperature field (Fig. 6c), is also
235 visible during the period of instrumental River Ammer discharge measurements (Fig. 5c).

236 During the period 1766–1870, the flood layer time-series shows also distinct decadal to multi-decadal
237 frequency variations (Fig. 7a) and higher flood layer frequencies during the second part of the 19
238 century, coincident with high flood frequencies in the greater Alpine region (Glur et al., 2013). Both
239 Z500 (Fig. 7b) and temperature (Fig. 7c) patterns during the period 1766–1870 are similar to the
240 corresponding patterns based on 20CR data for the period 1871–1999 (Fig. 6b and c).

241 **4. Discussion and conclusions**

242 We have shown that the majority of River Ammer floods (discharge higher than $125 \text{ m}^3\text{s}^{-1}$) is
243 associated with a pronounced ridge (trough) over the east Atlantic (western Europe), enhanced
244 moisture transport towards the Ammer catchment as well as relatively high potential vorticity at upper-
245 levels (200hPa). The upper-levels positive PV anomalies are associated with strong vertical motions, a
246 lowered tropopause and heavy precipitation in the Ammer region. Czymzik et al.(2010) have shown
247 that River Ammer flood events (discharge higher than $125 \text{ m}^3\text{s}^{-1}$) are related to specific atmospheric
248 circulation types. Five circulation types, as classified in the weather catalog of Gerstengarbe and
249 Werner (2005), could be attributed to more than one flood event during the period 1926–1999. Four of
250 the five atmospheric circulation types are compatible with a northwest to southeast or north to south
251 trajectory of cyclones crossing the Ammer region (Czymzik et al., 2010, their Fig. 10). This is

252 consistent with our IWT pattern and the corresponding 200hPa PV pattern associated to floods in the
253 instrumental River Ammer discharge record.

254 Floods over Europe are related with various moisture sources. For central European floods that occur in
255 June 2013, the main source of moisture was the land along the track of the three consecutive cyclones
256 that generated very high rainfall amounts in central Europe (Grams et al. 2014). Continental moisture
257 sources play also an important role for eastern European flood in May 2010, in addition to moisture
258 sources in the North Atlantic and Mediterranean (Winschall et al. 2014). Our analysis suggests that the
259 North Atlantic Ocean is the main moisture source for River Ammer floods. Therefore the flood layer
260 record from Lake Ammersee could be used to obtain information about patterns of moisture transport
261 from the North Atlantic towards Europe during the last millennia.

262 Under current climate conditions heavy precipitation in the Alpine region are associated with zonal
263 westerly or meandering circulation regimes, like e.g. the Vb cyclone track (e.g. Zängl, 2007). The Vb
264 track is characterized by low pressure systems moving northeastward from the Adriatic Sea into
265 continental Europe, causing orographic rainfall and potentially severe flooding along the Alpine crest
266 (e.g. Schlemmer et al., 2010) and in central Europe (Ionita et al., 2015). The synoptic scale pattern
267 associated to Ammer floods (Fig. 2a) is consistent with that provided by Schlemmer et al. (2010) and
268 Ionita et al. (2015). Moreover, it contains elements of the synoptic scale patterns associated to debris-
269 flow events in the southern Swiss Alps (Toreti et al., 2013). Glur et al. (2013) propose that a more
270 southerly and weaker subtropical high pressure zone favors the occurrence of Vb circulation patterns.
271 In particular, during the late 19th century which was characterized on average by cooler summers,
272 frequent Vb situations led to a higher frequency of floods in the Alpine region, coincident with higher
273 flood frequencies in the Ammer region. The high flood frequency of River Ammer, as derived from
274 both, River Ammer discharge and Lake Ammersee flood layer data is related with increased frequency
275 of southerly intrusions of high PV favoring strong vertical motions and heavy rainfall in the region.

276 However, higher River Ammer flood frequencies are recorded during colder conditions over western
277 and central Europe and warmer conditions in Eastern Europe (Fig. 5). Cooler conditions over western
278 and central Europe are induced by enhanced advection of relatively cold air from the northwest while
279 warmer conditions over northeastern Europe are related to a flow of warm air from the southeast (Fig.
280 5). Another forcing factor for positive temperature anomalies over northeastern Europe is the negative
281 cloudiness anomalies which dominate this region during high flood frequency periods (not shown).

282 Heavy precipitation and floods in the Alps region variability was related to various atmospheric
283 teleconnection patterns, like the North Atlantic Oscillation (Swierczynski et al., 2012), the North
284 Atlantic Oscillation and East Atlantic pattern (Toreti et al., 2013) and the Summer North Atlantic
285 Oscillation (Peña et al., 2015). The atmospheric circulation anomaly pattern associated to River Ammer
286 flood projects well on the negative phase of the East Atlantic-Western Russia (EA-WR) pattern, a 3-
287 center east– west wave-train with one center of action close to the British islands, one in northeast
288 China, and one centre with an opposite sign near the Caspian sea (e.g. Barnston and Livezey, 1987).

289 Indeed, the analysis of annual EA-WR index based on 20CR data reveals that the frequency of the
290 negative phase of the EA-WR pattern is significantly higher than the frequency of its positive phase
291 during River Ammer flood years from 1871 to –1999 (not shown). Therefore, the Lake Ammersee
292 flood layer record might provide the chance to reconstruct changes in the polarity of the EA-WR during
293 the late Holocene. An addition, we conclude that the Lake Ammersee flood layer record (Czymzik et
294 al., 2010, 2013) might be used to deduce information about past change in specific moisture transport
295 and atmospheric circulation patterns. In particular, the flood layer record from varved Lake Ammersee
296 sediments can be used to reconstruct the frequency of high potential vorticity intrusions over Western
297 Europe during last millennia.

298

299 *Acknowledgements.* This study is promoted by Helmholtz funding through the Polar Regions and
300 Coasts in the Changing Earth System (PACES) program of the AWI. Funding by the Helmholtz
301 Climate Initiative REKLIM and the Excellence Cluster Marum (OC3 “The Ocean in the Earth System”
302 High- and low-latitude atmosphere–ocean interactions) are gratefully acknowledged. M.Czymzik was
303 partly funded by the Swedish Research Council (VR grant to RM:Dnr:2013–8421). We thank the data
304 contributors for making their data available to the public.

305

306

307

308

309

310

311

312

313

314

315

316

317

318

319

320

321

322

323 **References**

- 324 Barnston, A. G. and Livezey, R. E.: Classification, seasonality and persistence of low-frequency
325 atmospheric circulation patterns, *Mon. Weather Rev.*, 115, 1083–1126, 1987.
- 326 Bayerisches Landesamt für Umwelt: Daily River Ammer runoff data from 1926 to 2006, Munich,
327 Germany, 2007.
- 328 Browning, K. A.: The dry intrusion perspective of extra-tropical cyclone development, *Meteorol.*
329 *Appl.*, 4, 317–324, 1997.
- 330 Casty, C., Raible, C. C., Stocker, T. F., Luterbacher, J. and Wanner, H.: A European pattern
331 climatology 1766–2000, *Clim. Dyn.*, 29, 791–805, doi:10.1007/s00382-007-0257-6, 2007.
- 332 Compo, G. P., Whitaker, J. S., Sardeshmukh, P.D., Matsui, N., Allan, R.J., Yin, X., Gleason, B.E.,
333 Vose, R.S., Rutledge, G., Bessemoulin, P., Brönnimann, S., Brunet, M., Crouthamel, R., Grant,
334 A.N., Groisman, P. Y., Jones, P. D., Kruk, M. C., Kruger, A. C., Marshall, G. J., Maugeri, M.,
335 Mok, H. Y., Nordli, Ø., Ross, T. F., Trigo, R. M., Wang, X. L., Woodru, S. D., and Worley, S.
336 J.: The Twentieth Century Reanalysis Project, *Q. J. Roy. Meteor. Soc.*, 137, 1–28,
337 doi:10.1002/qj.776, 2011.
- 338 Corella, J. P., Benito, G., Rodriguez-Lloveras, X., Brauer, A., and Valero-Garcés, B. L.: Annually-
339 resolved lake record of extreme hydro-meteorological events since AD 1347 in NE Iberian
340 Peninsula, *Quaternary Sci. Rev.*, 93, 77–90, doi:10.1016/j.quascirev.2014.03.020, 2014.
- 341 Czymzik, M., Dulski, P., Plessen, B., von Grafenstein, U., Naumann, R., and Brauer, A.: A 450 year
342 record of spring-summer flood layers in annually laminated sediments from Lake Ammersee
343 (southern Germany), *Water Resour. Res.*, 46, W11528, doi:10.1029/2009WR008360, 2010.
- 344 Czymzik, M., Brauer, A., Dulski, P., Plessen, B., von Grafenstein, U., Naumann, R., and Scheffler, R.:
345 Orbital and solar forcing of shifts in Mid- to Late Holocene flood intensity from varved

346 sediments of pre-alpine Lake Ammersee (southern Germany), *Quaternary Sci. Rev.*, 61, 96-110,
347 2013.

348 Dee, D. P., Uppala, S. M., Simmons, A. J., Berrisford, P., Poli, P., Kobayashi, S., Andrae, U., Bal-
349 maseda, M. A., Balsamo, G., Bauer, P., Bechtold, P., Beljaars, A. C. M., van de Berg, L., Bidlot,
350 J., Bormann, N., Delsol, C., Dragani, R., Fuentes, M., Geer, A. J., Haimberger, L., Healy, S. B.,
351 Hersbach, H., Hólm, E. V., Isaksen, L., Kållberg, P., Köhler, M., Matricardi, M., McNally,
352 A. P., Monge-Sanz, B. M., Morcrette, J.-J., Park, B.-K., Peubey, C., de Rosnay, P., Tavolato, C.,
353 Thépaut, J.-N., and Vitart, F.: The ERA-interim reanalysis: configuration and performance of the
354 data assimilation system, *Q. J. Roy. Meteor. Soc.*, 137, 553–597, doi:10.1002/qj.828, 2011.

355 Gerstengarbe, F.-W., and Werner, P. C.: *Katalog der Grosswetterlagen Europas (1881–2004) nach*
356 *Paul Hess and Helmut Brezowsky, verbesserte and ergänzte Auflage, Rep. Issue 6, Potsdam Inst.*
357 *For Clim. Impact Res., Potsdam, Germany, 2005.*

358 Glur, L., Stefanie, B. W., Buntgen, U., Gilli, A., Haug, G. H., Schar, C., Beer, J., and Anselmetti, F.
359 S.: Frequent floods in the European Alps coincide with cooler periods of the past 2500 years,
360 *Scientific Reports*, 3, 2770, doi:10.1038/srep02770, 2013.

361 Grams, C.M., Binder, H., Pfahl, S., Piaget, N., Wernli, H.: Atmospheric processes triggering the central
362 European floods in June 2013, *Nat. Hazards Earth Syst. Sci.*, 14, 1691–1702,
363 doi:10.5194/nhess-14-1691-2014,2014.

364 Hoskins, B. J., Draghici, I., and Davies, H. C.: A new look at the Ω -equation. *Q. J. Roy. Meteor Soc.*,
365 104, 31–38, 1978.

366 Ionita, M., Lohmann, G., and Rimbu, N.: Prediction of spring Elbe discharge based on stable
367 teleconnections with winter global temperature and precipitation, *J. Climate*, 21, 6215–6226,
368 2008.

369 Ionita, M., Lohmann, G., Rimbu, N., and Chelcea, S.: Interannual variability of Rhine River
370 streamflow and its relationship with large-scale anomaly patterns in spring and autumn, *J.*
371 *Hydrometeorol.*, 13, 172–188, 2012.

372 Ionita, M., Dima, M., Lohmann, G., Scholz, P., and Rimbu, N.: Predicting the June 2013 European
373 flooding based on precipitation, soil moisture and sea level pressure, *J. Hydrometeorol.*, 16,
374 598–614, doi:10.1175/JHM-D-14-0156.1, 2015.

375 Jacobeit, J., Glaser, R., Luterbacher, J., and Wanner, H.: Links between flood events in central Europe
376 since AD 1500 and large-scale atmospheric circulation modes, *Geophys. Res. Lett.*, 30, 1172,
377 doi:10.1029, 2003.

378 Krichak, S. O., Breitgand, J. S., Gualdi, S., and Feldstein, S.: Teleconnection–extreme precipitation
379 relationships over the Mediterranean region, *Theor. Appl. Climatol.*, 117, 679–
380 692, doi:10.1007/s00704-013-1036-4, 2014.

381 Lavers, D. A., Villarini, G., Allan, R. P., Wood, E. F., and Wade, A. J.: The detection of atmospheric
382 rivers in atmospheric reanalysis and their links to British winter floods and the large-scale
383 climatic circulation, *J. Geophys. Res.*, 117, D20106, doi:10.1029/2012JD018027, 2012.

384 Ludwig, R., Tascher, S., and Mauser, W.: Modelling floods in the Ammer catchment: limitations and
385 challenges with a coupled meteo-hydrological model approach, *Hydrol. Earth Syst. Sci.*, 7,
386 833–847, 2013.

387 Peña, J. C., Schulte, L., Badoux, A., Barriendos, M., and Barrera-Escoda, A.: Influence of solar
388 forcing, climate variability and modes of low-frequency atmospheric variability on summer
389 floods in Switzerland, *Hydrol. Earth Syst. Sci.*, 19, 3807–3827, doi:10.5194/hess-19-3807-
390 2015, 2015.

391 Petrow, T., and Merz, B.: Trends in flood magnitude frequency and seasonality in Germany in the
392 period 1951–2002, *J. Hydrol.*, 371, 129–141, doi:10.1016/j.hydrol.2009.03.024, 2009.

393 Schillereff, D., Chiverrell, R., Macdonald, N., and Hooke, J.: Flood stratigraphies in lake sediments: a
394 review, *Earth-Sci. Rev.*, 135, 17–37, doi:10.1016/j.earscirev.2014.03.011, 2014.

395 Schlemmer, L., Martius, O., Sprenger, M., Schwierz, C., and Twitchett, A.: Disentangling the forcing
396 mechanisms of heavy precipitation event along the Alpine south side using potential vorticity
397 inversion, *Mon. Weather Rev.*, 138, 2336–2353, doi:10.1175/2009MWR3202.1, 2010.

398 Swierczynski, T., Brauer, A., Lauterbach, S., Martín-Puertas, C., Dulski, P., von Grafenstein, U., and
399 Rohr, C.: A 1600 yr seasonally resolved record of decadal-scale flood variability from the
400 Austrian Pre-Alps, *Geology*, 40, 1047–1050, 2012.

401 Toreti, A., Xoplaki, E., Maraun, D., Kuglitsch, F. G., Wanner, H., and Luterbacher, J.:
402 Characterization of extreme winter precipitation in Mediterranean coastal sites and associated
403 anomalous atmospheric circulation patterns, *Nat. Hazards Earth Syst. Sci.*, 10, 1037–1050,
404 doi:10.5194/nhess-10-1037-2010, 2010.

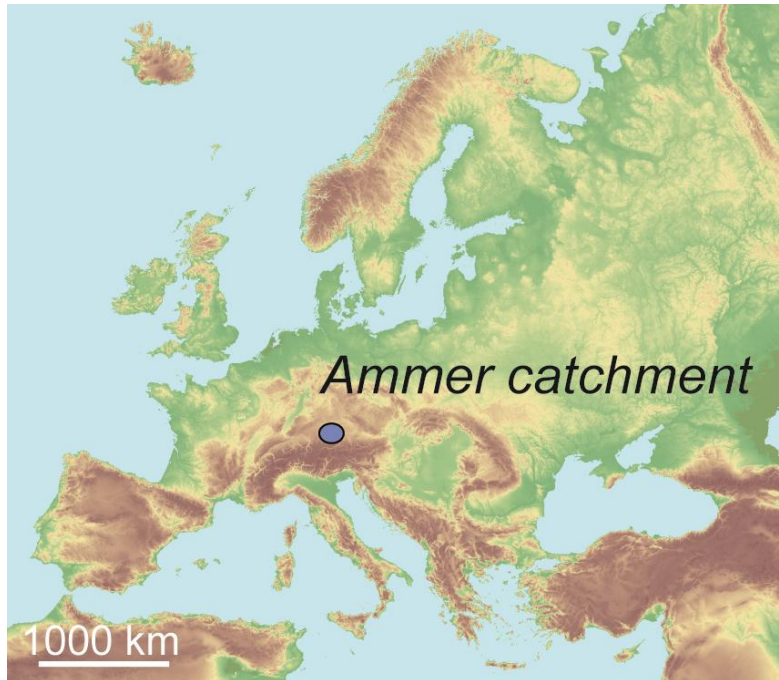
405 Toreti, A., Schneuwly-Bollschweiler, M., Stoffel, M., and Luterbacher, J.: Atmospheric forcing of
406 debris flows in the southern Swiss Alps, *J. Appl. Meteorol. Clim.*, 52, 1554–1560,
407 doi:10.1175/JAMC-D-13-077.1, 2013.

408 Zängl, G.: Interaction between dynamics and cloud microphysics in orographic precipitation
409 enhancement: a high-resolution modeling study of two North Alpine heavy-precipitation events,
410 *Mon. Weather Rev.*, 135, 2817–2840, 2007.

411 Zolina, O., Simmer, C., Kapala, A., Gulev, S., and Maechel, H.: Seasonally dependent changes of
412 precipitation extremes over Germany since 1950 from a very dense observational network, *J.*
413 *Geophys. Res.-Atmos.*, 113, D06110, doi:10.1029/2007JD008393, 2008.

414 Winschall, A., Pfahl, S., Sodemann, H., and Wernli, H.: Comparison of Eulerian and Lagrangian
415 moisture source diagnostics –the flood event in eastern Europe in May 2010, *Atmos. Chem.*
416 *Phys.*, 14, 6605–6619, doi:10.5194/acp-14-6605-2014, 2014.

a)



b)

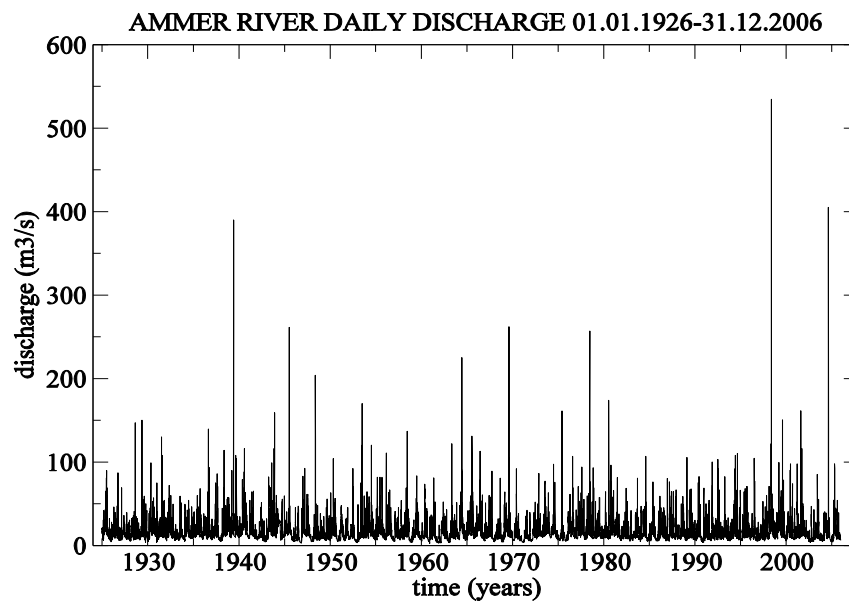
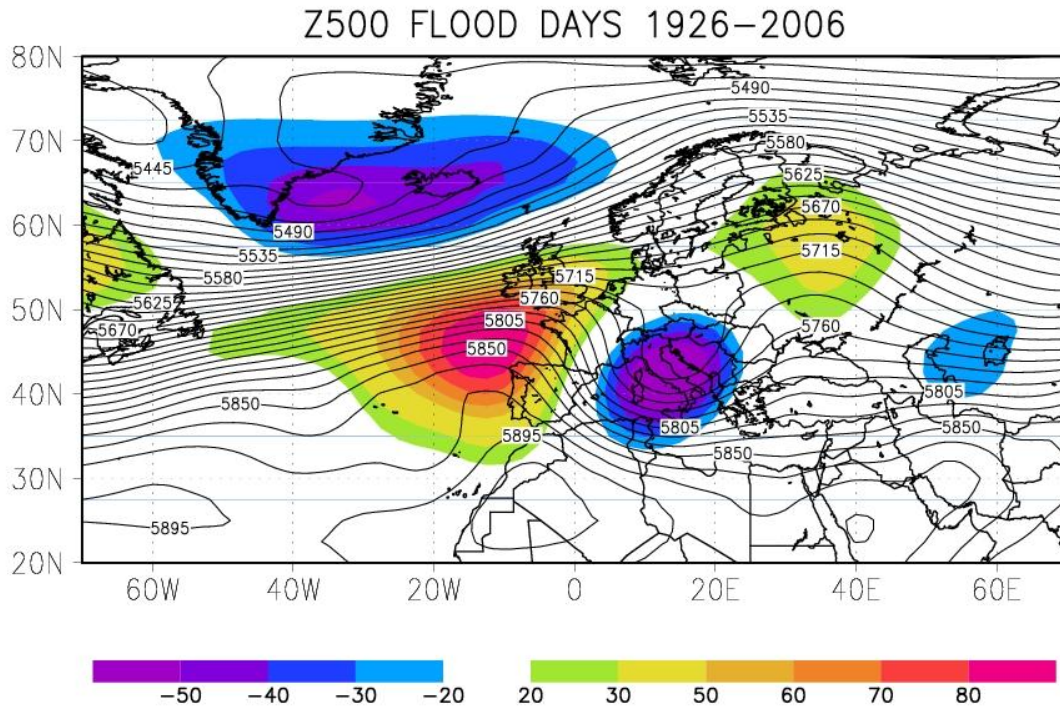


Figure 1. (a) Geographical location of the Ammer catchment and (b) time series of the observed mean daily River Ammer runoff during the period 1926–2006.

417
418
419
420
421
422
423

a)



b)

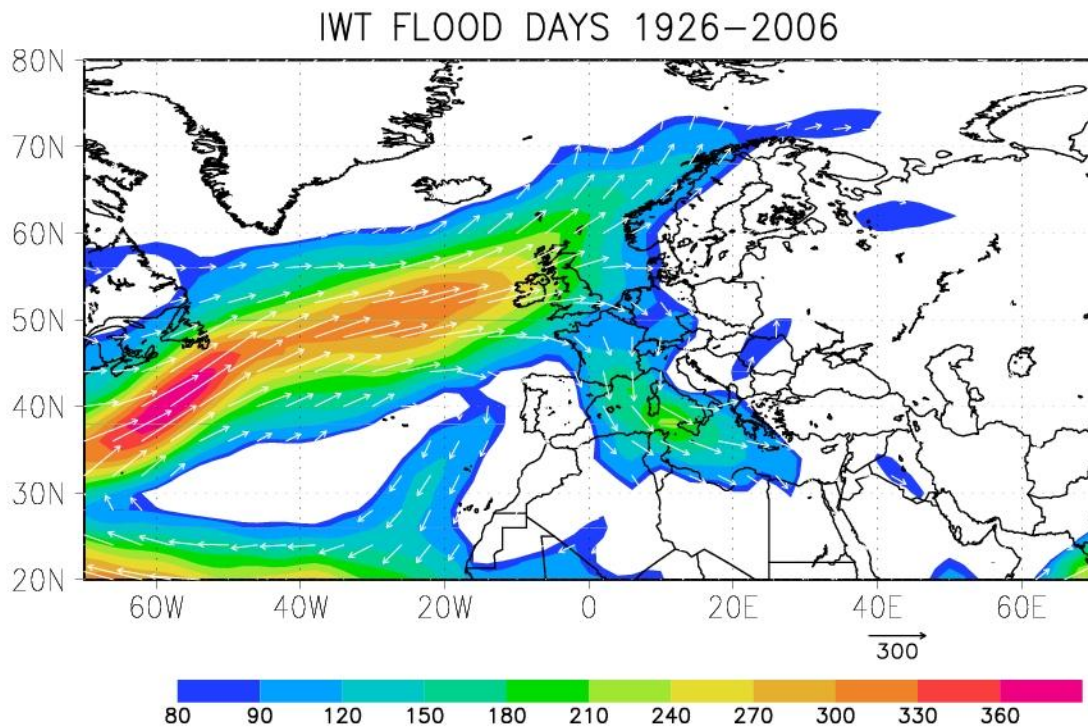
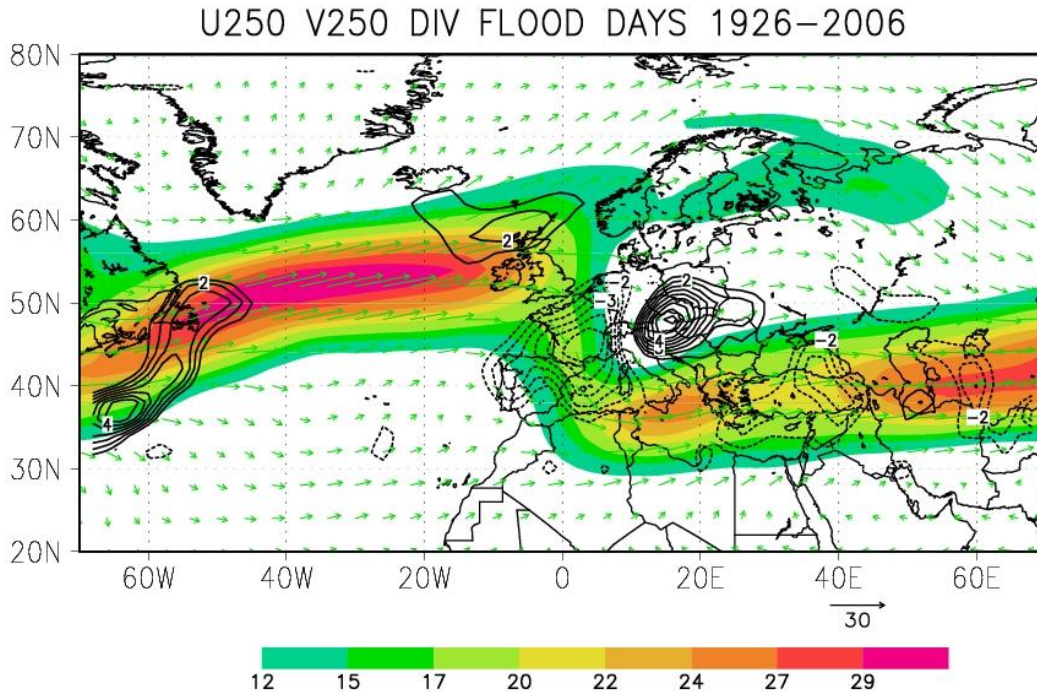


Figure 2. (a) Composite map of daily 500hPa geopotential height (contour) and anomalies (shaded) corresponding to River Ammer floods (discharge higher than $125 \text{ m}^3 \text{ s}^{-1}$) for the period 1926–2006 and (b) composite map of IWT for flood days (vector) and its magnitude (color). Units: Z500 (m) and IWT ($\text{kg m}^{-1} \text{ s}^{-1}$).

a)



b)

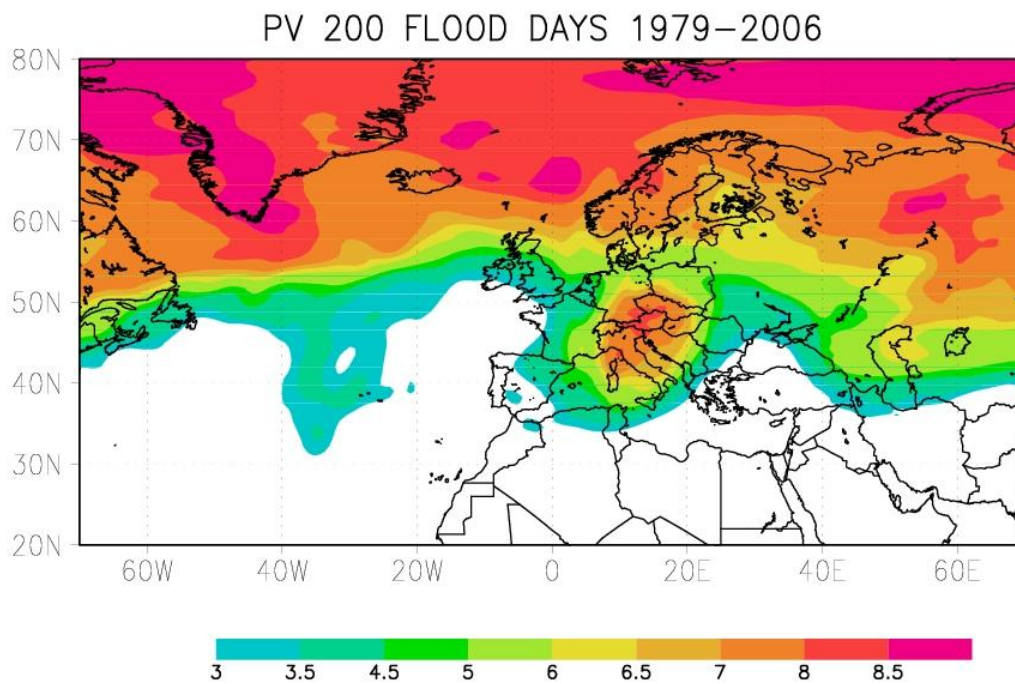


Figure 3. Composite map of (a) the 250hPa wind (vector), its magnitude (color) and divergence (contour) for Ammer flood days for the period 1926–2006 and (b) composite map of 200hPa potential vorticity for flood days during 1979–2006.

Units: U250 (m s^{-1}), divergence (10^{-6} s^{-1}) and potential vorticity (PVU).

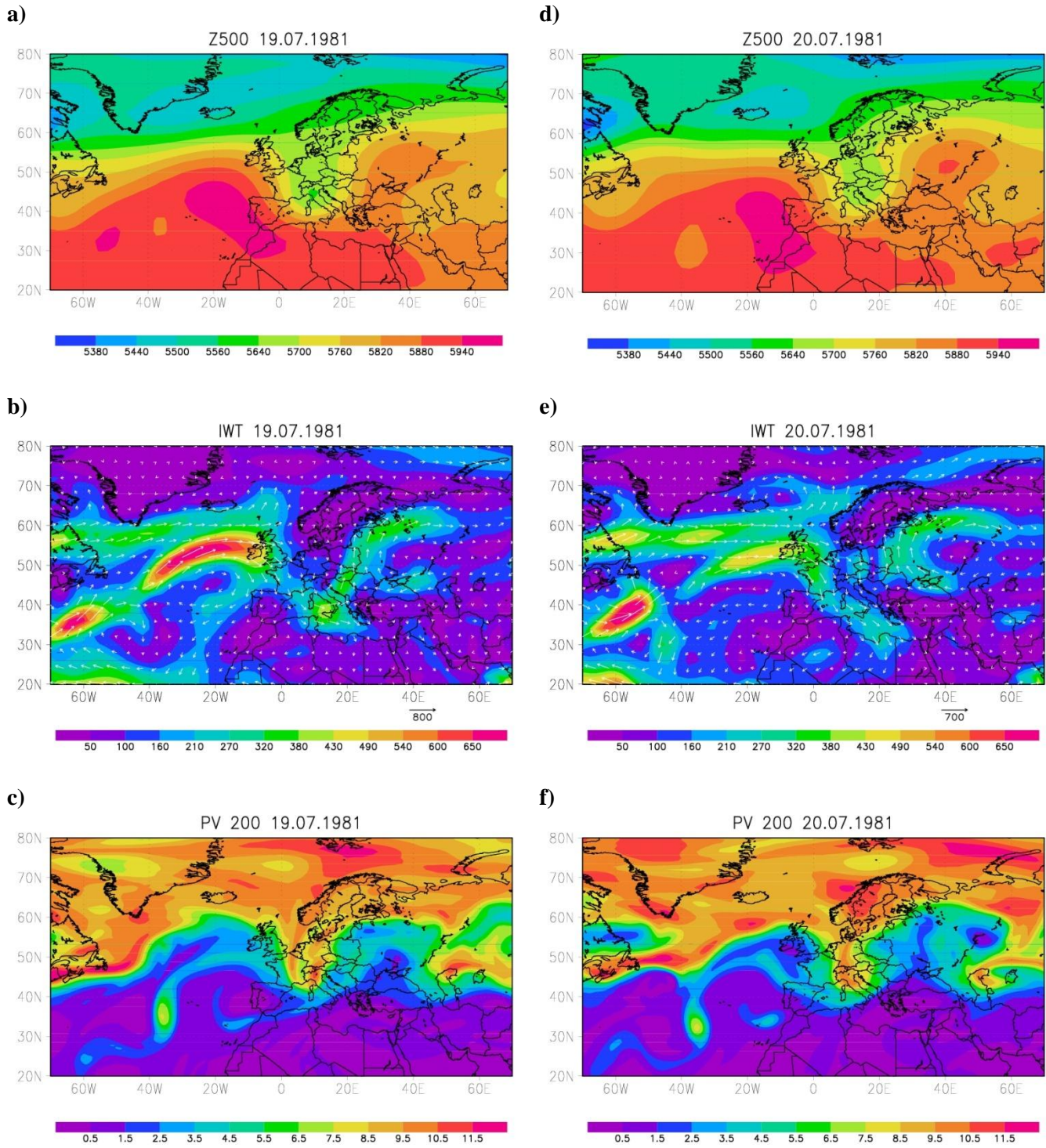
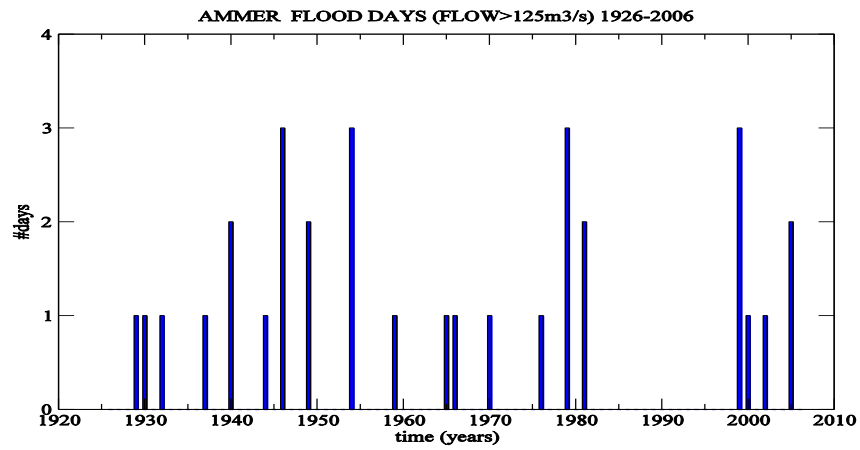


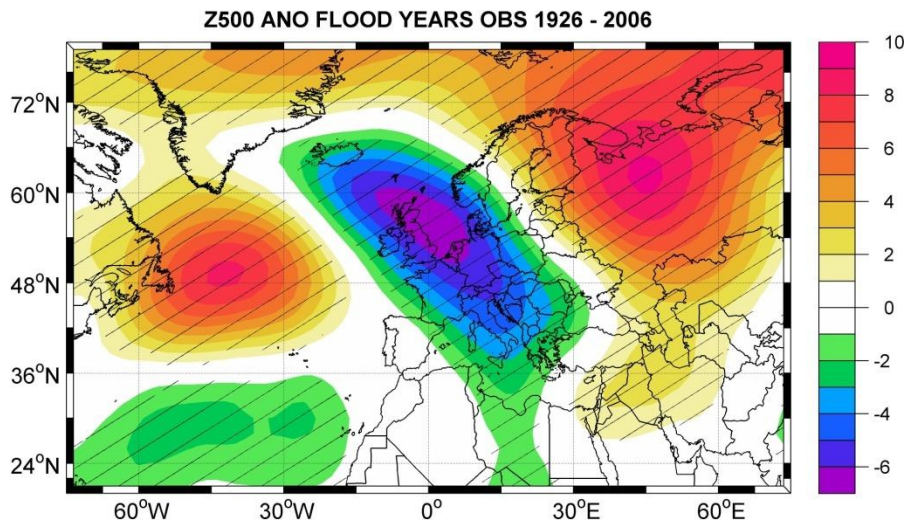
Figure 4. Synoptic-scale meteorology during the River Ammer flood days 19 and 20 June 1981: **(a)** Z500, **(b)** IWT and **(c)** PV for 19 June 1981; **(d)**, **(e)** and **(f)** as in **(a)**, **(b)** and **(c)** but for 20 June 1981. Units: Z500 (m), IWT ($\text{kg m}^{-1} \text{s}^{-1}$) and PV (PVU).

427
428
429
430

a)



b)



c)

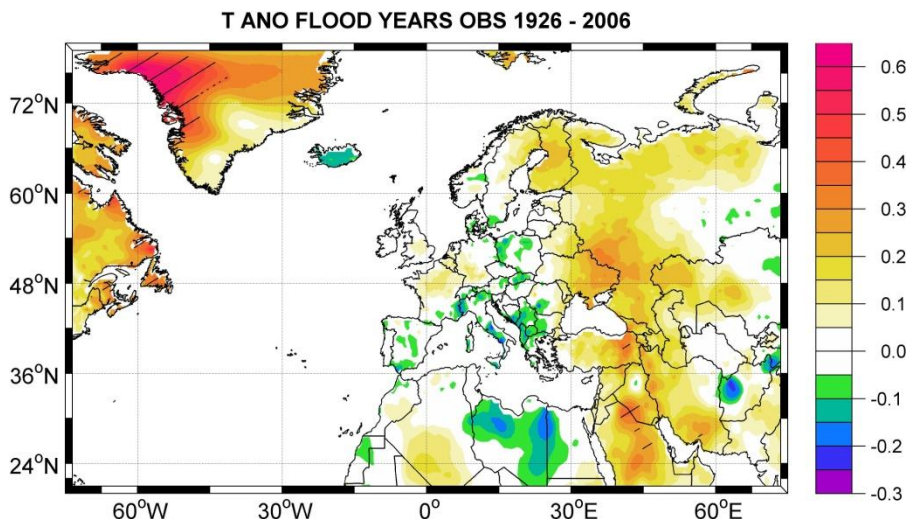
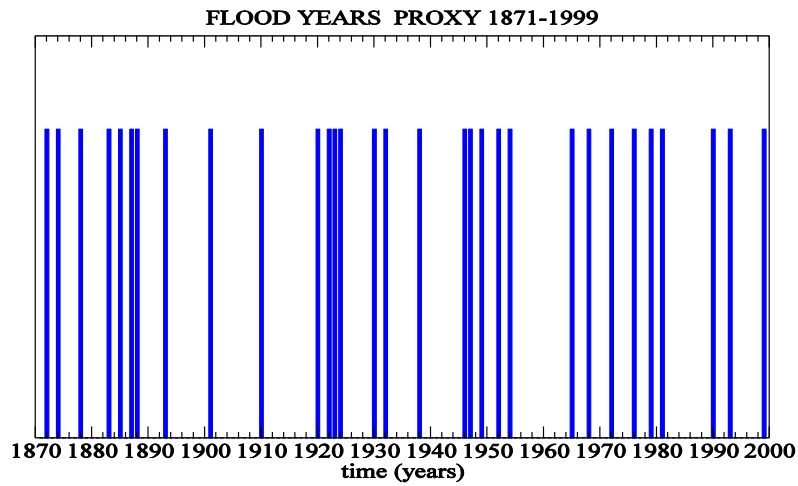
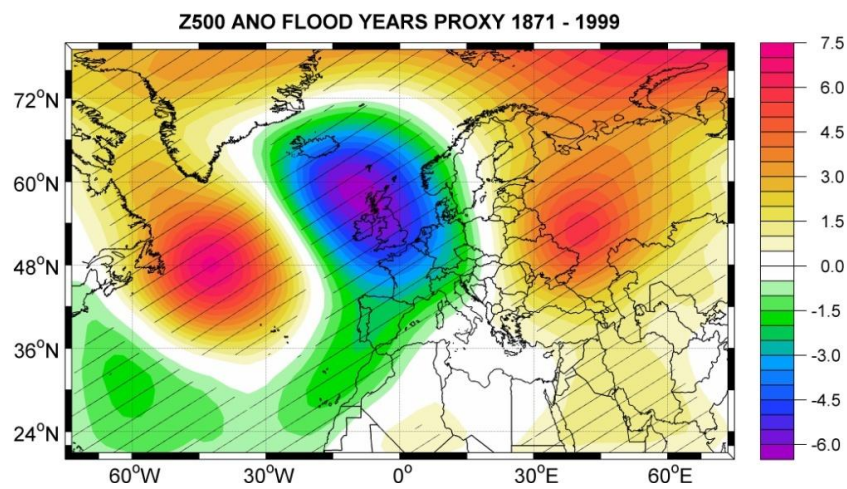


Figure 5. (a) Observed River Ammer flood frequency (daily discharge higher than $125 \text{ m}^3 \text{ s}^{-1}$) and (b) composite map of Z500 and (c) air temperature anomalies for flood years. Hatched regions: anomalies significantly different from zero (90% level). Units: Z500 (m) and T ($^{\circ}\text{C}$).

a)



b)



c)

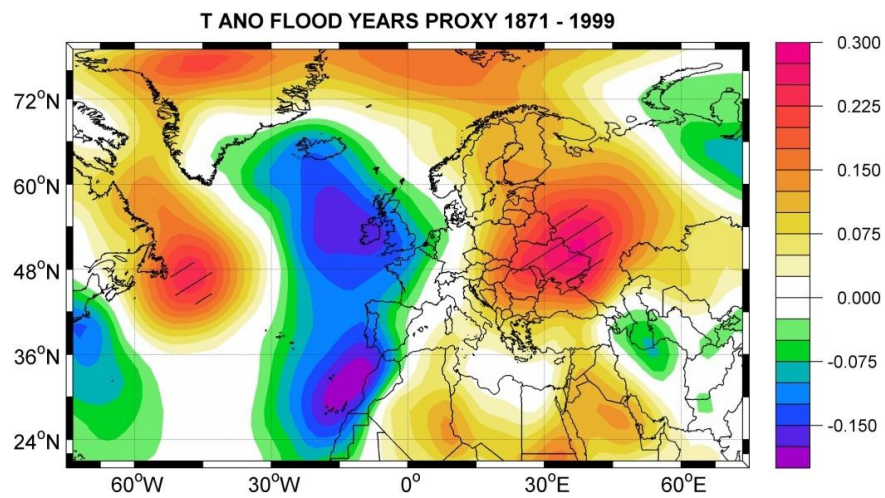
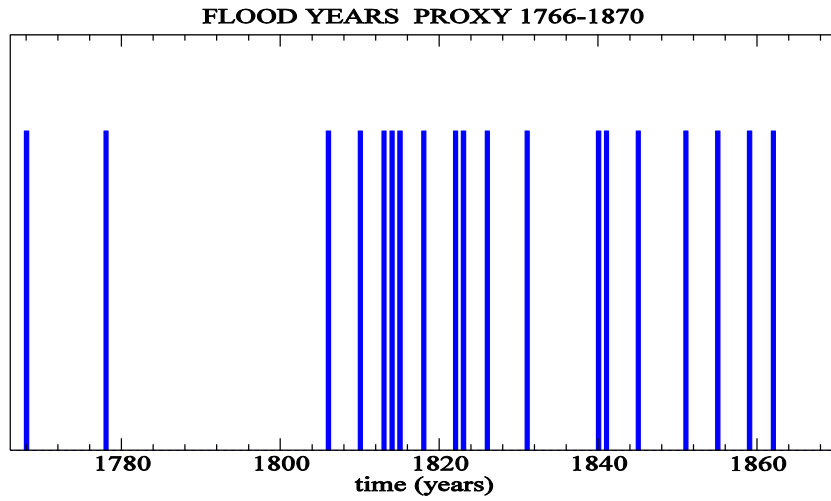


Figure 6. (a) River Ammer flood layer record for the period 1871–1999 (see text for details). Vertical bars depict years with flood layer. Composite map of (b) Z500 and (c) T anomalies for years with flood layer as shown in (a).

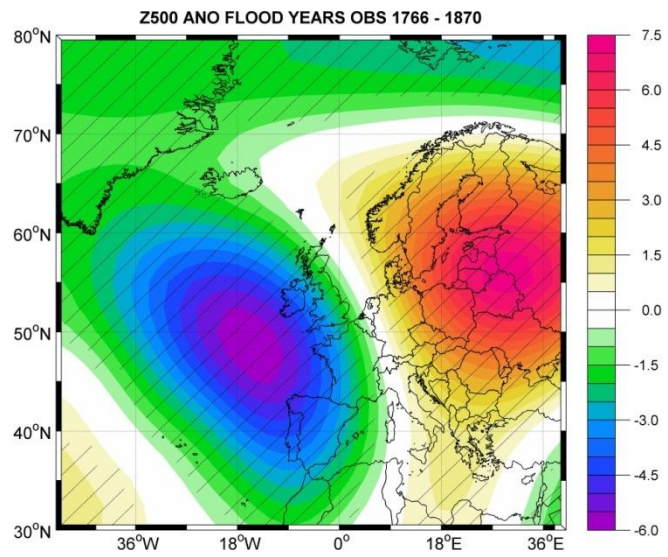
Hatched regions: anomalies significantly different from zero (90% level).

Units: Z500 (m) and T (°C).

a)



b)



c)

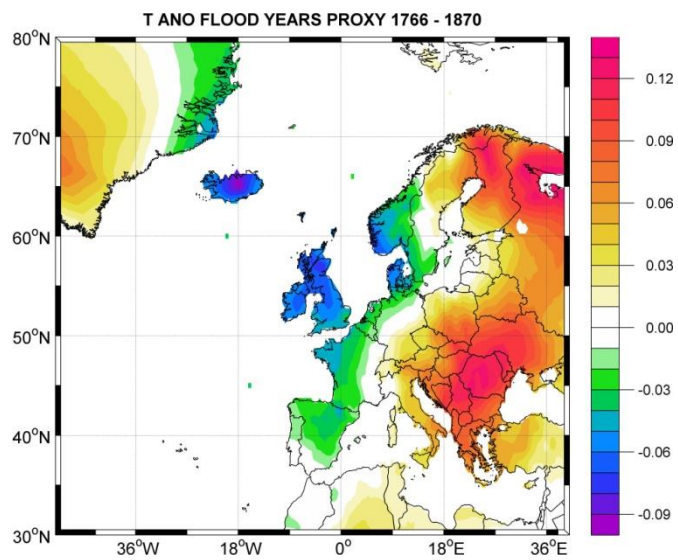


Figure 7. Same as in Figure 6) but for the 1766–1870.